Applied Surface Science 258 (2012) 6943–6951

Contents lists available at SciVerse ScienceDirect

Applied Surface Science

journal homepage: www.elsevier.com/locate/apsusc

Pilot-scale production of mesoporous silica-based adsorbent for CO_2 capture

Hou Chuan Wang[a], Chungsying Lu[b,*], Hsunling Bai[c], Jyh Feng Hwang[a], Hsiu Hsia Lee[a], Wang Chen[a], Yuhao Kang[a], Shing-Ting Chen[a], Fengsheng Su[b], Shih-Chun Kuo[b], Fang-Chun Hu[b]

[a] Green Energy and Environment Research Laboratories, Industrial Technology Research Institute, Hsinchu 310, Taiwan
[b] Department of Environmental Engineering, National Chung Hsing University, Taichung 402, Taiwan
[c] Institute of Environmental Engineering, National Chiao Tung University, Hsinchu 300, Taiwan

ARTICLE INFO

Article history:
Received 3 October 2011
Received in revised form 17 February 2012
Accepted 23 March 2012
Available online 31 March 2012

Keywords:
Amine modification
CO_2 adsorption
Spherical mesoporous silica particles
Pilot-scale

ABSTRACT

This study presents a pilot-scale spray drying system designed to manufacture spherical mesoporous silica particles (MSP) that is capable of producing up to 100 g per hour. The MSP fabricated via a nozzle pressure of 4 kg/cm^2 and a drying temperature of 200 °C possess a high specific area of 1012 m^2/g, a narrow pore size distribution with an average pore diameter of 2.4 nm, and large pore volume of 0.81 cm^3/g. They were further modified with a tetraethylenepentamine (TEPA-MSP) to enhance CO_2 adsorption selectivity from gas streams. The adsorption capacity of 15% CO_2 on TEPA-MSP was significantly influenced by adsorption temperature and water vapor of air streams, and reached a maximum of 87.05 mg/g (1.98 mmol/g) at 60 °C and 129.19 mg/g (2.94 mmol/g) at a water vapor of 6.98%. The adsorption capacities and the physicochemical properties of TEPA-MSP were preserved through 20 cycles of adsorption–desorption operation. A comparative study revealed that the TEPA-MSP had better adsorption performance of 15% CO_2 than the TEPA-modified granular activated carbon and zeolite. These results suggest that the TEPA-MSP can be stably employed in the prolonged cyclic CO_2 adsorption and that they possess good potential for CO_2 capture from flue gas.

1. Introduction

The issue of global warming caused by the burning of fossil fuels has attracted much attention after the Kyoto Protocol came into effect on February 16, 2005. Taiwan emitted approximately 265 million tons of carbon dioxide (CO_2) into the atmosphere in 2006 [1]. The major anthropogenic sources of CO_2 emission include coal-fired power plants, steel plants, and cement plants.

Application of CO_2 capture, utilization, and storage (CCUS) technologies on flue gas is considered to be a useful method of lessening global warning [2]. Several CO_2 capture technologies including absorption, adsorption, cryogenics, membranes and so forth, have been developed [3,4]. Among them, the design of a full-scale adsorption process might be feasible and therefore the development of a promising material that would adsorb CO_2 with a high capacity and able to be regenerated with low energy input will undoubtedly enhance the competitiveness of an adsorptive separation system in a flue gas application [5]. Low-temperature solid adsorbents reported in the literature [6,7] include physical adsorbents (carbon-based materials [8–12], zeolites [13–20] and metal organic frameworks [21–25]), amine-loaded carbons [26–30] and amine-loaded silicas [31–41]. Even though each family of adsorbents has its advantage; most of them were manufactured in the laboratory-scale system and commonly have an output of only several milligrams per hour. Therefore, it is necessary to increase the production rate of these adsorbents and test their performance on CO_2 adsorption before they can be employed in practical field applications.

The spray drying system provides a simple means to continuously manufacture mesoporous silica materials, and it can be preceded at a wide range of industrial production scale. Several studies have been conducted to investigate the effects of spray-drying parameters such as the surfactant concentration, the water fraction and the gas flow on the properties of mesoporous silica materials in the laboratory-scale production [42–44]. However, limited researches have been carried out on MSPs synthesized by the pilot-scale spray drying system for the CO_2 adsorption.

In this study, the spherical mesoporous silica particles (MSP) was manufactured by a pilot-scale spray drying system and further modified by tetraethylenepentamine ($H_2NC_2H_4NHC_2H_4NHC_2H_4NHC_2H_4NH_2$, abbreviated as TEPA) to enhance their adsorption selectivity of CO_2 from gas streams in the 30–70 °C. Cyclic CO_2 adsorption on TEPA-MSP via a thermal/vacuum swing operation was conducted to evaluate their repeated availability in the prolonged cyclic CO_2 adsorption. Effects of water vapor in the gas stream on CO_2 adsorption were also investigated and discussed.

* Corresponding author. Tel.: +886 4 22852483; fax: +886 4 22862587.
E-mail address: clu@nchu.edu.tw (C. Lu).

0169-4332/$ – see front matter © 2012 Elsevier B.V. All rights reserved.
http://dx.doi.org/10.1016/j.apsusc.2012.03.140

2. Materials and methods

2.1. Preparation of the adsorbents

Precursors were prepared by dissolving tetraethyl orthosilicate (TEOS), cetyltrimethyl ammonium bromide (CTAB), ethanol, and hydrochloric acid (HCl) into deionized water and then stirring the mixture for 30 min. TEOS was used as the silica source while CTAB was used as the structure-directing template. The molar composition of the precursors was TEOS: 0.18 CTAB: 10 ethanol: 0.008 HCl: 40 H_2O [45,46].

Fig. 1 shows a schematic diagram of the pilot-scale spray drying system for manufacture of MSP. The pilot-scale spray drying system consists of (1) a spray drying reactor for the nebulization of precursors, (2) a reaction tower for the self-organization of particles by solvent evaporation, and (3) a cyclone and a bag filter for collection of products. The droplet diameters of sprayed precursor were in 7–8 μm when the flow rate of liquid precursor and the flow rate of compressed air were controlled at 15 mL/min and 150 L/min, respectively. The nozzle pressure was evaluated in 2–5 kg/cm^2 range while the drying temperatures of reaction tower for solvent removal from the self-organizing particles were tested in 150–250 °C. The resulting MSP were carried by clean air, passed through a HEPA filter at 1.5 m^3/min, and collected by the cyclone or bag filter. Finally, the collected MSP were calcined at 550 °C for 4 h in a muffle furnace to remove the surfactant template. This fabrication method is capable of producing calcined MSP at a rate of 100 g per hour.

Five grams of MSP were dispersed into flasks containing TEPA solution (5 g of 99% TEPA + 50 g of ethanol). After the mixture was stirred for 2 h at room temperature and filtered through a 0.45 μm fiber filter, the filtrated solid was removed to an oven to evaporate ethanol at 80 °C for 10 h and then evaporate water at 100 °C for 2 h. Finally, the mixture was pretreated by purging pure N_2 gas in a furnace at 80 °C for 2 h to extract water and ethanol molecules from the inner pores of MSP. Thermal analyses of MSP before and after TEPA modification by a thermogravimetric analyzer (TGA) indicated that the amount of TEPA grafted on the final product was about 50 wt%. Different TEPA-loaded MSP samples were also prepared by the same modification procedure.

To compare the CO_2 adsorption performance of MSP with other commercially available adsorbents, granular active carbon (GAC, BPL, Calgon Carbon Co., China) and mordenite zeolite (CBV21, Zeolyst International, USA) were selected because of their wide use for the removal of volatile organic compounds from waste gases. The surface area, pore volume, and average pore diameter, respectively, are 969 m^2/g, 0.2 cm^3/g and 2.6 nm for GAC and 214 m^2/g, 0.16 cm^3/g, and 40 nm for zeolite. They were functionalized with the TEPA mixture under the same modification procedure.

2.2. Adsorption experiments

The CO_2 adsorption experiments were conducted in a cylindrical Pyrex glass column having a total height of 16 cm and an internal diameter of 1.27 cm. The column was filled with 5.0 g of adsorbents equivalent to a packing height of 7 cm and placed within a temperature-controlled furnace. Because the best location for CO_2 adsorption in a coal-fired power plant to take place is after the flue gas desulfurization (FGD) and before the stack [3], the tested temperature was selected from 30 to 70 °C (in 10 °C increments), which covers the typical temperature range of 45–55 °C in the post-FGD. The SO_2 and NO_X concentrations in the post-FGD were low (typically less than 100 ppmv) and their effects on CO_2 adsorption were thus not considered. The gas stream was kept dry with the exception of during the moisture effect study, in which the water vapor range of 0–17.4 vol% was tested at 60 °C. The selection of this water vapor range nearly covers the typical range of 8–12% in the flue gas [47]. Wet flow was obtained by dispersing the gas stream through a humidifier in which water bath was controlled at 60 °C.

Compressed air was first passed through a silica gel air dryer to remove moisture and oil and was then passed through a HEPA filter (Gelman Science, Ann Arbor, MI) to remove particulates. Two mass flow controllers (MKS Instruments Inc., Andover, MA) were employed to control the influent CO_2 concentration by regulating the flow rates of pure CO_2 and clean air (diluting gas) entering the mixing chamber. The influent and effluent gas streams were passing through a CO_2 analyzer for online measurement and the associated concentrations (C_{in} and C_{eff}) were expressed in terms of percent in volume. All of the experiments were repeated twice, and only the mean values were reported.

The C_{in} was in the range of 5–50%, which was selected to be representative of different CO_2 concentrations in combustion gases from many kinds of industrial activities such as coal-fired power plants (12–14%), cement plants (14–33%) [48], or coal gasification system (30–35%) [49]. The influent flow rate (Q_{in}, L/min) was controlled at 0.1 L/min equivalent to an empty-bed retention time of 12.2 s. The adsorption capacity of CO_2 (q_t, mg/g) at a certain time (t, min) was estimated as

$$q_t = \frac{1}{m}\int_0^t (Q_{in}C_{in} - Q_{eff}C_{eff})dt \quad (1)$$

where m is the dry weight of virgin adsorbents (g) and Q_{eff} is the effluent gas flow rate (L/min). Integrating Eq. (1) from $t = 0$ to equilibrium time (t_e) when C_{eff} reaches C_{in} gives the equilibrium capacity of the adsorbents (q_e, mg/g). Blank tests (without adsorbents) were also conducted with various C_{in}. The q_t of the blank was eliminated from the q_t of the adsorbents.

2.3. Cyclic adsorption experiments

The adsorption process was operated at 60 °C and with a C_{in} of 15%. As the CO_2 adsorption reached equilibrium, the q_e was measured. A combination of thermal desorption at 75 °C and vacuum desorption at 0.145 atm was used by changing the influent gas to purified air and operating the system at 0.08 L/min for 240 min. Thermal desorption utilizes heat to increase the evaporation of CO_2 such that they can be removed (separated) from the surface of spent adsorbents while vacuum desorption with purified air creates a pressure/concentration gradient that induces adsorbed CO_2 to be removed from the surface of spent adsorbents. Cyclic CO_2 adsorption on TEPA-MSP was conducted for 20 cycles of adsorption-regeneration operation.

2.4. Analytical methods

CO_2 concentration was measured using a CO_2 analyzer (Model 2820, Bacharach Inc., UK). The surface morphologies of the adsorbents were characterized via a field emission scanning electron microscope (SEM, model JEOL JSM-6700, Tokyo, Japan) and a high-resolution transmission electron microscopy (TEM, model JEOL JEM-2010, Tokyo, Japan). The physical properties of the adsorbents were determined by N_2 adsorption/desorption at 77 K via a Micromeritics ASAP 2020 volumetric sorption analyzer (Norcross, GA). N_2 adsorption/desorption isotherms were measured at a relative pressure (P_{N2}/P_0) range of 0.0001–0.99 and employed to determine surface area, pore volume, and average pore diameter via the Barrett–Johner–Halenda (BJH) equation for pore size of 1.7–100 nm. The crystal phase of the adsorbents was characterized by a powder X-ray diffractometer (XRD, Mac Science Co. Ltd., Japan) using Cu Kα radiation (40 kV, 30 mA). The thermal stability of the adsorbents was determined by a TGA (TGA i1000, Instrument

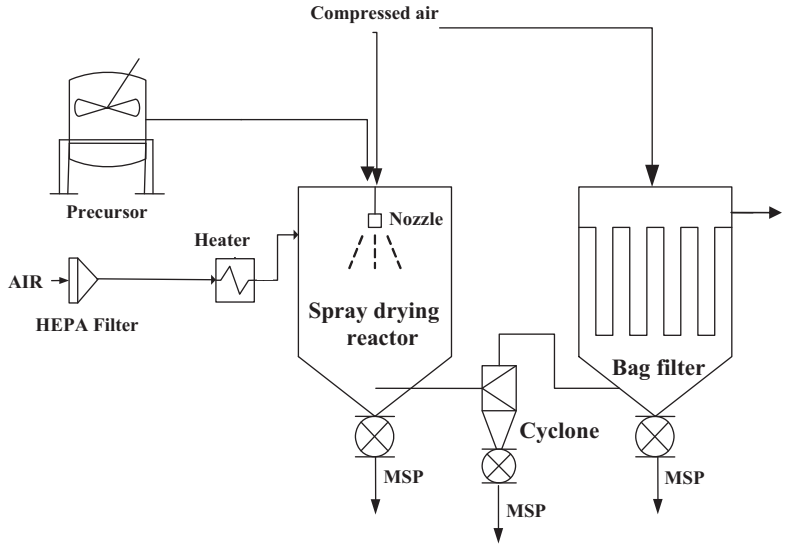

Fig. 1. Diagram of the pilot-scale system for manufacture of MSP.

Specialists Inc., Twin Lakes, WI) at a heating rate of 10 °C/min from 30 to 800 °C. The surface functional groups of the adsorbents were evaluated by a Fourier transform infrared (FTIR) spectrometer (Spectrum 100FTIR Spectrometer, PerkinElmer, Waltham, MA) using the KBr method. The temperature and water vapor in the gas stream was measured by a temperature/relative humidity sensor (Rotronic Hygromer M130D, Rotronic Co., Ltd., Zurich, Switzerland).

3. Results and discussion

3.1. Characterizations of MSP and TEPA-MSP

Nozzle pressure and drying temperature are important operating parameters to synthesize MSP in the spray-drying process [50] and their effects on the morphology of MSP were evaluated by SEM analysis (Fig. 2). It is seen from Fig. 2(a) and (b) that hollow, mushroom-like deformed and crushed particles were formed at nozzle pressures of 2 and 3 kg/cm^2. However, if the nozzle pressure increased to 4 or 5 kg/cm^2, nearly spherical particles were formed as shown in Fig. 2(c) and (d). When the drying temperature of 250 °C was employed, disrupted particles were observed in Fig. 2(e) likely because of rapid solvent evaporation [51], which show lower surface area and smaller pore volume than those fabricated at a drying temperature of 200 °C.

Table 1 reports the physical properties of MSPs fabricated via various nozzle pressures and drying temperatures and their corresponding equilibrium adsorption capacity (q_e) of 15% CO_2 at 60 °C. It is clear that the nozzle pressure showed insignificant effects on surface area, pore volume and average pore diameter of MSP. However, the average particle size of MSP decreased from 8.7 to 3.0 μm as the nozzle pressure increased from 2 to 5 kg/cm^2 at a drying temperature of 200 °C. The physical properties of MSP appeared to have no direct correlation with the drying temperature but the MSP fabricated via a drying temperature of 200 °C displayed higher surface area, pore volume and average pore diameter than those fabricated via drying temperatures of 150 and 250 °C. The q_e of MSP increased with the nozzle pressure in 2–4 kg/cm^2 but decreased with the nozzle pressure in 4–5 kg/cm^2. The q_e of MSP fabricated via a drying temperature of 200 °C was much higher than those fabricated via drying temperatures of 150 and 250 °C likely because of higher surface area, pore volume and average pore diameter.

Above results indicated that the MSP fabricated via nozzle pressure of 4 kg/cm^2 and drying temperature of 200 °C (Sample no. 3) not only possess good physical properties but also give the highest q_e and they were thus selected as CO_2 adsorbents to further study their physicochemical properties and cyclic CO_2 adsorption.

Fig. 3 exhibits the TEM images of MSP and TEPA-MSP. As observed from Fig. 3(a) and the previous SEM image of Fig. 2(c), the morphology of MSP is in well shaped spherical particles with particle sizes ranged from a few hundred nanometers to several micrometers. The structure of well-ordered MSPs can be seen from Fig. 3(b), which shows self-assembled hexagonal structure. The pore channels of MSP were constructed and arranged in a two-dimensional orientation to fit into the spherical shape of MSP during the self-assembly stage. After TEPA modification, the TEM image shown in Fig. 3(c) reveals less obvious mesopore structure because TEPA was occupied on the surface of MSP.

Fig. 4 exhibits the pore size distributions of MSP and TEPA-MSP. It is noted that the pore volumes of MSP and TEPA-MSP mainly appeared in the pore size of 2–3 nm and 1–3 nm, respectively. This reflects that both samples have narrow pore size distribution.

Fig. 5 presents the N_2 adsorption/desorption isotherm curves of MSPs and TEPA-MSP. It is evident that the TEPA-MSP showed lower adsorption capacities of N_2 than the MSP, reflecting that less amounts of porosity within TEPA-MSP likely because of the grafting of TEPA on their surface. The isotherm curves of MSP displayed a type IV shape based on IUPAC classification [52], exhibiting a rapid rise in N_2 adsorption capacity up to a P/P_0 of 0.35, which is the evidence of capillary condensation of N_2 molecules in the primary mesopores. This is typical characteristics for mesoporous solid particles. The isotherm curves of TEPA-MSP are approximately type I, which is classified as the Langmuir type adsorption and is characterized by the formation of a complete monolayer. After an increase up to a P/P_0 of 0.02, the isotherm curves exhibit a small increment with P/P_0, indicating a narrow pore size distribution. The adsorption and desorption curves coincide with each other, implying the absence of adsorption hysteresis [53].

Surface area, pore volume, and average pore diameter respectively are 1012 m^2/g, 0.81 cm^3/g, and 2.40 nm for MSP and 91.33 m^2/g, 0.057 cm^3/g, and 2.49 nm for TEPA-MSP. It is noted that surface area and pore volume of MSP significantly decreased after TEPA modification, probably because of the partial blockage of pore entrance by the formation of amine functional groups on their

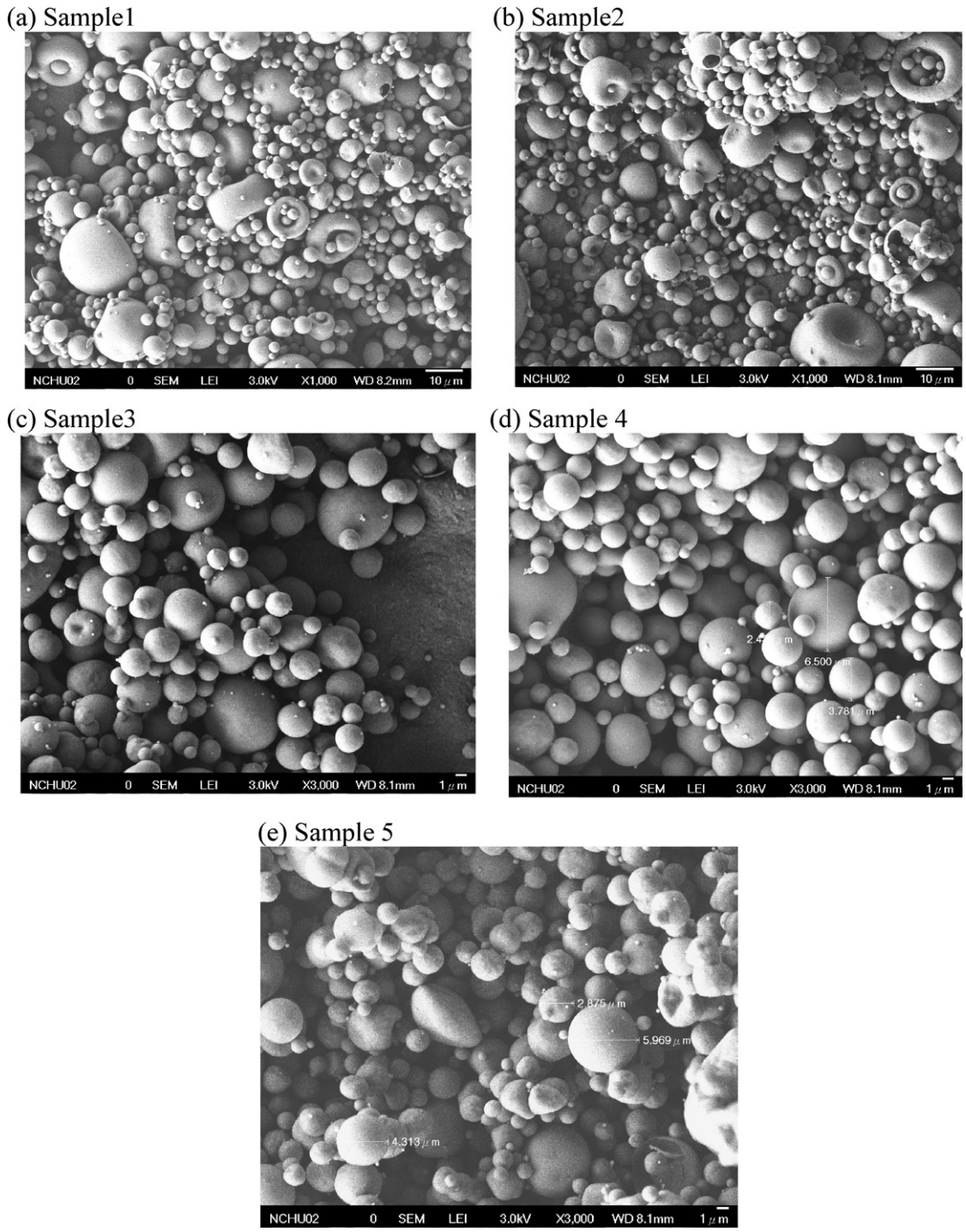

Fig. 2. SEM images of MSP manufactured under various nozzle pressures and drying temperatures. (a) $P = 2$, (b) $P = 3$, (c) $P = 4$, (d) $P = 5$ kg/cm^2 at 200 °C, and (e) $P = 4$ kg/cm^2 at 250 °C.

Table 1
Effects of nozzle pressure and drying temperature on the physical properties of MSP and their adsorption capacities of CO_2.

Sample no.	Nozzle pressure (kg/cm^2)	Drying temperature (°C)	S_{BET} (m^2/g)	V_P (cm^3/g)	d_{BJH} (nm)	Average particle size (μm)	q_e (mg/g)
1	2	200	1010	0.82	2.5	8.7	4.5
2	3	200	1008	0.80	2.5	7.5	5.5
3	4	200	1012	0.81	2.4	3.2	7.0
4	5	200	1008	0.79	2.4	3.0	6.3
5	4	150	948	0.54	2.1	–	1.6
6	4	250	920	0.35	2.0	3.1	1.5

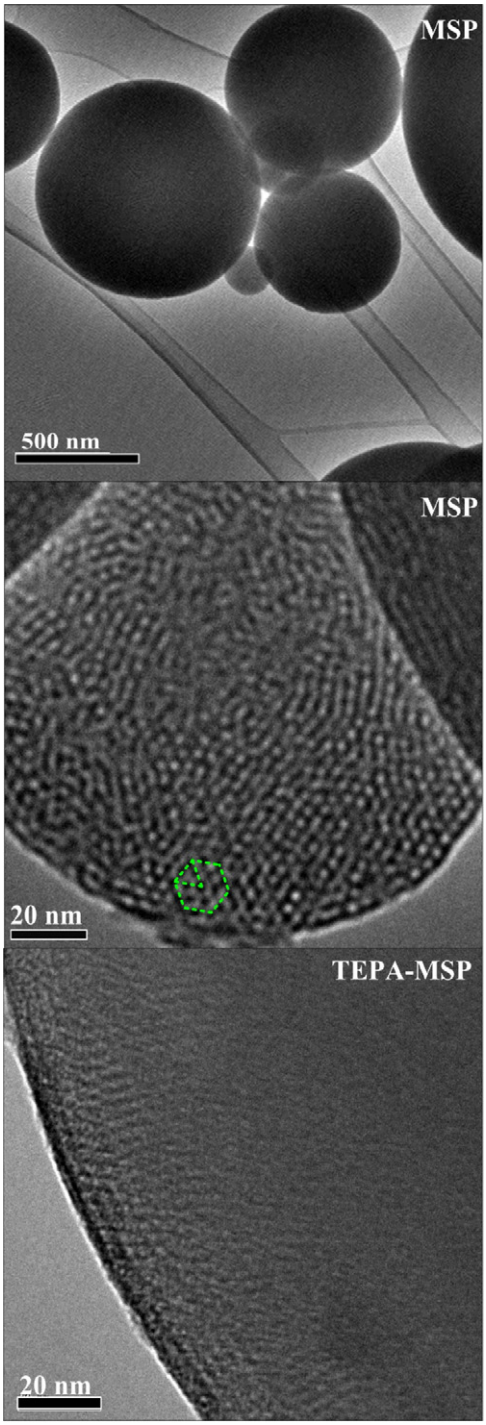

Fig. 3. TEM images of MSP and TEPA-MSP. Image on the top is the enlargements of the TEM image.

external and internal surface. Similar findings have been reported in the literature for various amine-modified silica adsorbents [36].

Fig. 6 displays the XRD patterns of MSP and TEPA-MSP. The (1 0 0) diffraction peak located at $2\theta = 2.8–3.0^{\circ}$ are clearly observed for both samples, indicating the evidence of ordered mesoporous structure [45]. The intensity of the diffraction peak became weaker after TEPA modification probably because of layers of TEPA grafted on their surface that reduced their well ordered-pore structure.

Fig. 7 presents the TG profiles of MSP and TEPA-MSP. The TG profile of MSP showed a weight loss close to 5% below 110 °C, which could be attributed to the evaporation of adsorbed water. As

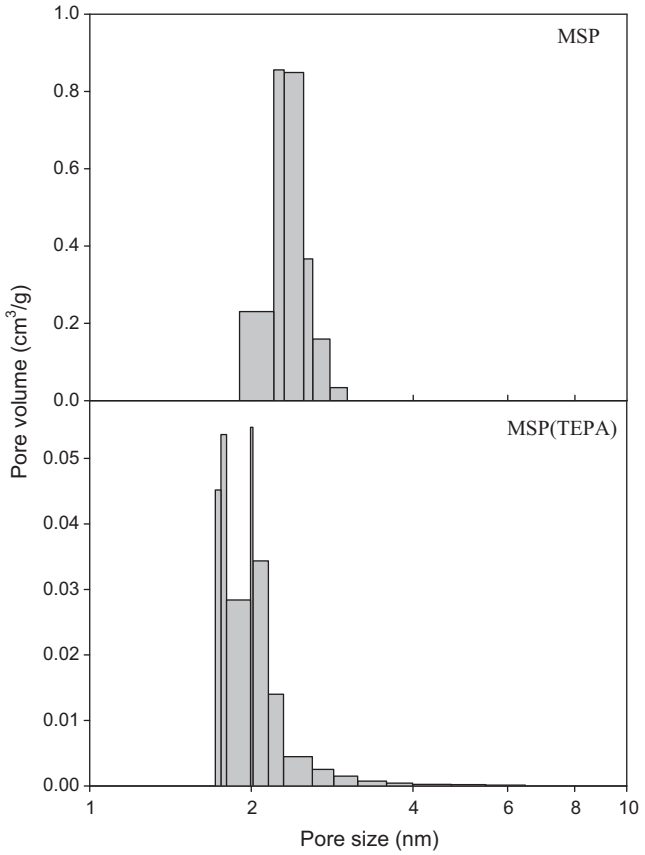

Fig. 4. Pore size distributions of MSP and TEPA-MSP.

the temperature exceeded 110 °C, the weight loss became insignificant and a remaining weight of 93.8% was observed at 800 °C. The TEPA-MSP had a broader temperature range for weight loss, and exhibited four main weight loss regions. The first weight loss region (<80 °C) is due to the evaporation of adsorbed water. The second region (80–185 °C) displayed a remarkable weight loss, which can be mainly attributed to the volatilization or thermal degradation of TEPA [54]. The third region (185–700 °C) shows a weight loss of approximately 20% because of the carbon-chain (C—H_2) decomposition accompanied by oxidation processes. After temperature exceeded 700 °C, the weight loss became small (<0.2%)

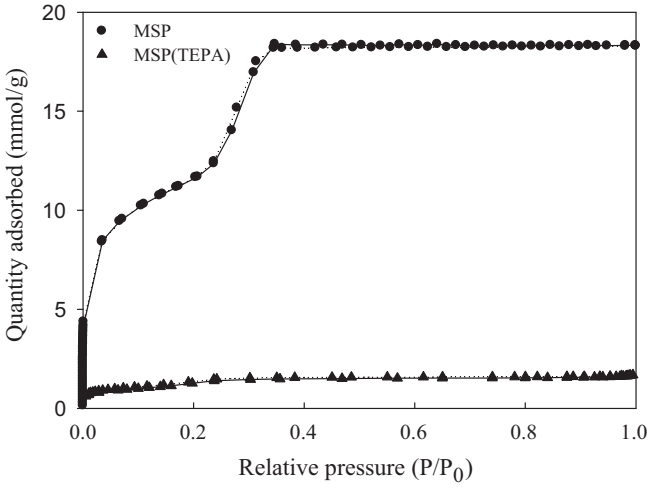

Fig. 5. Nitrogen adsorption (solid line) and desorption (dash line) isotherms of MSP and TEPA-MSP.

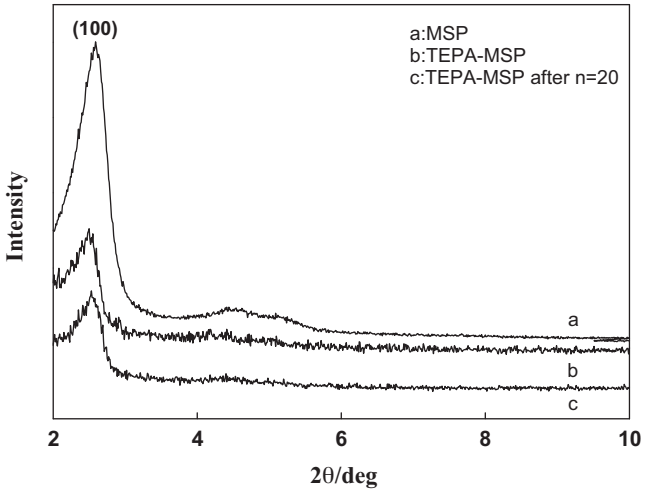

Fig. 6. XRD patterns of MSP and TEPA-MSP.

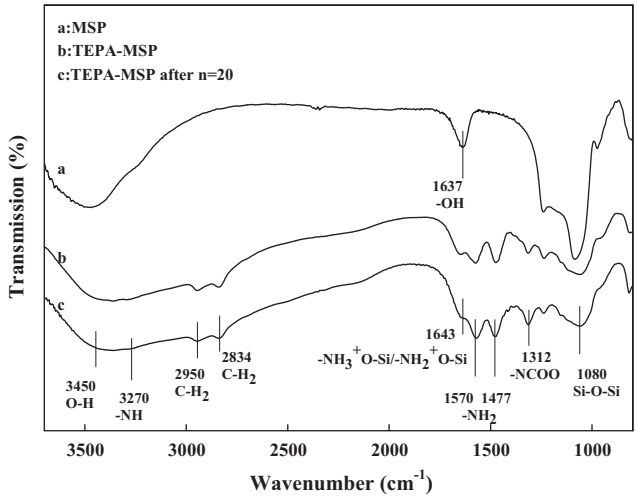

Fig. 8. IR spectra of MSP and TEPA-MSP.

and a remaining weight of 46.1% was obtained at 800 °C. The TEPA demonstrated thermal stability up to 80 °C, suggesting that regeneration of spent TEPA-MSP should be conducted at temperatures below 80 °C.

Fig. 8 shows the IR spectra of MSP and TEPA-MSP. The IR spectrum of MSP displays significant bands at 3450, 1637, and 1080 cm^{-1}. These bands are related to O—H stretching vibrations of the hydrogen-bonded silanol groups, H—O—H bend, and Si—O—Si asymmetric stretching vibrations, respectively [55,56]. The IR spectrum of TEPA-MSP exhibits significant bands at 3450, 3270, 2950, 2834, 1643, 1570, 1477, 1312, and 1080 cm^{-1}. The bands at 2950 and 2834 cm^{-1} can be attributed to C—H_2 stretching from CH_2CH_2—NH_2 groups, while the bands at 1570 and 1477 cm^{-1} are related to N—H_2 vibration in the primary amine group (RNH_2) [31,56,57]. The band at 3270 cm^{-1} is related to N—H vibration in the secondary amine group (R_2NH). The band at 1643 cm^{-1} is associated with the NH_3^+ deformation of the protonated primary amine group or secondary amine group (—NH_3^+O—Si/—NH_2^+O—Si), which is the product of amine group interacted with silanol group (Si—OH) on the MSP surface [56]. The presence of the C—H_2, N—H_2, N—H,—NH_3^+O—Si/—NH_2^+O—Si, and decreased O—H at 3450 cm^{-1} after TEPA modification confirms that the TEPA has been grafted on the MSP surface. The band at 1312 cm^{-1} can be attributed to weakly adsorbed gaseous CO_2 [31,56].

3.2. CO_2 adsorption

Fig. 9 shows the q_e of 15% CO_2 adsorption on various TEPA-loaded MSPs at 60 °C. It is seen that the q_e of MSP was 7.03 mg/g and remarkably enhanced to 63.25, 87.05, and 81.98 mg/g with 40, 50, and 60 wt% TEPA-loaded MSP, respectively. Although surface area and pore volume of MSP were much higher than those of TEPA-MSP, the q_e of MSP was remarkable lower than those of TEPA-loaded MSP. This could be explained by the fact that that the introduction of TEPA to the MSP surface significantly improved the CO_2 adsorption selectivity of CO_2 from gas stream probably because of the increase of surface amine groups as shown in Fig. 8. The maximum q_e of MSP was obtained at a TEPA load of 50 wt%, which was approximately 12 times the q_e of MSP. The decrease in q_e after the further increase of TEPA load from 50 to 60 wt% could be because of the mass transfer limitation caused by the deposition of excessive TEPA on the external MSP surface resulting in the resistance of CO_2 diffusion into the inter-pores of MSP. A similar finding for CO_2 adsorption on polyethylenimine-modified MCM-41 has been reported in the literature [58]. Thus, 50 wt% TEPA-loaded MSP were selected to further study the CO_2 adsorption from gas stream.

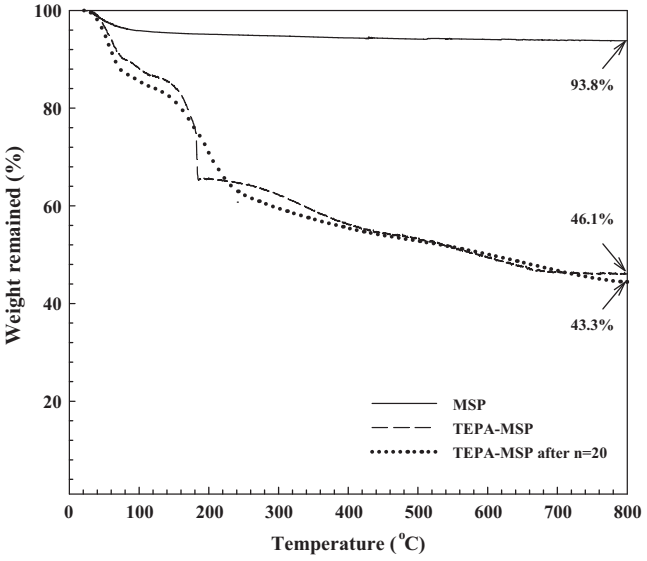

Fig. 7. TGA profiles of MSP and TEPA-MSP.

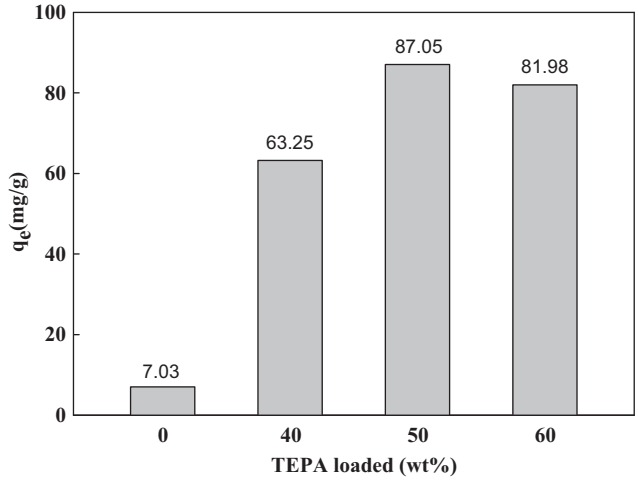

Fig. 9. Equilibrium capacities of 15% CO_2 adsorption on various TEPA-loaded MSPs at 60 °C.

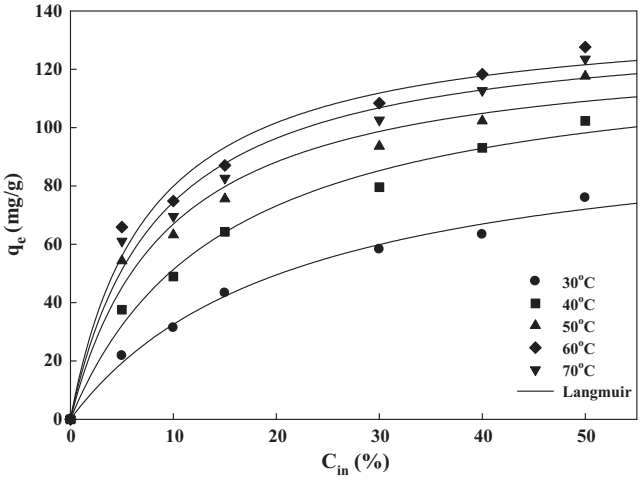

Fig. 10. Adsorption isotherms of CO_2 with TEPA-MSP in the 30–70 °C range.

Fig. 10 exhibits the CO_2 adsorption isotherms of TEPA-MSP in the 30–70 °C. Symbols represent the measured data while solid lines depict Langmuir isotherms. It is evident that the q_e increased with C_{in} and the temperature in the 30–60 °C but slightly decreased with the temperature in the 60–70 °C. The maximum q_e appeared at 60 °C. Raising the temperature from 30 to 60 °C increased the molecular flexibility of TEPA loaded in the mesopore channels of MSP, which might partly contribute to the increase of q_e at higher temperatures [56]. However, further raising the temperature to 70 °C led to a decrease in q_e probably because of the decrease of the chemical interaction and van der Waals' force between CO_2 molecules and the TEPA-MSP surface. Similar observations on the correlation of q_e with temperature had been reported in other studies of amine-loaded SBA-15 [56] and MCM-41 [32,33], which revealed a maximum q_e at 75 °C. This may be due to the nature of silica adsorbents. The q_e at 30, 40, 50, 60, and 70 °C are, respectively, 43.27, 64.26, 75.59, 87.05, and 82.64 mg/g with a C_{in} of 15% and 75.32, 102.14, 117.63, 127.62, and 123.56 mg/g with a C_{in} of 50%.

The constants of Langmuir equation (q_m and b) were obtained from fitting the measure q_e in Fig. 10 to Langmuir equation and the results are given in Table 2. The correlation coefficients (r^2) are in 0.922–0.991, indicating that the adsorption isotherms of CO_2 on TEPA-MSP could be described by Langmuir adsorption model. The q_m, which represents the adsorption capacity of CO_2, increased with the temperature and reached a maximum of 145.6 mg/g (3.31 mmol/g) at 60 °C. The constant b, which is associated with the heat of CO_2 adsorption, exhibited the same trend as q_m, reflecting the highest affinity between CO_2 and TEPA-MSP at 60 °C.

3.3. Effects of water vapor in the gas stream

Effects of water vapor on adsorption of 15% CO_2 on TEPA-MSP were investigated at 60 °C. The q_e of TEPA-MSP at water vapor of 0, 3.49, 6.98, 10.47, 13.96 and 17.45% were 87.05, 97.53, 129.19, 106.84, 99.17 and 97.20 mg/g, respectively. It is evident that the presence of water vapor in the gas stream significantly influences the CO_2 adsorption on TEPA-MSP. The q_e increased from 87.05 to 129.19 mg/g as the water vapor increased from 0 to 6.98% but decreased from 129.19 to 99.17 mg/g as the water vapor further increased from 6.98 to 17.45%. The maximum q_e appeared at a water vapor of 6.98%.

There are two possible reasons to explain a rise in q_e with water vapor of gas stream. First, TEPA contains primary amine (RNH_2) and secondary amine (R_2NH); both amines can react with CO_2 and lead to the formation of a carbamate ion ($RNHCOO^-$ or R_2NCOO^-). The presence of water vapor then hydrolyzes the carbamate ion to regenerate amine molecule and form bicarbonate ion (HCO_3^-) [56]. Second, the amine molecules can also directly react with CO_2 and H_2O to form bicarbonate ion. The decrease in q_e with water vapor of gas stream might be explained by the competitive adsorption between CO_2 and H_2O at the same adsorption sites [33].

Table 2
Constants of Langmuir equation for 15% CO_2 adsorption on TEPA-MSP at various temperatures.

Temperature (°C)	q_m (mg/g)	b (L/mg)	r^2
30	103.4	0.0025	0.991
40	127.2	0.0039	0.989
50	139.1	0.0052	0.959
60	145.6	0.0068	0.922
70	142.6	0.0061	0.927

Note: Langmuir equation: $q_e = q_m bC_e/1 + bC_e$.

3.4. Cyclic CO_2 adsorption

Evaluating the stability of TEPA-MSP during extensive adsorption–desorption cycles is required to determine the frequency of their replacement. The adsorption index (abbreviated as AI, %) was calculated as the percentage ratio of the q_e of the regenerated adsorbents to the virgin adsorbents, thus 100% AI implies that the sorbent has not deteriorated at all.

Fig. 11 shows the q_e and their associated AI of TEPA-MSP during 20 cycles of adsorption–desorption operation (n). It is observed that

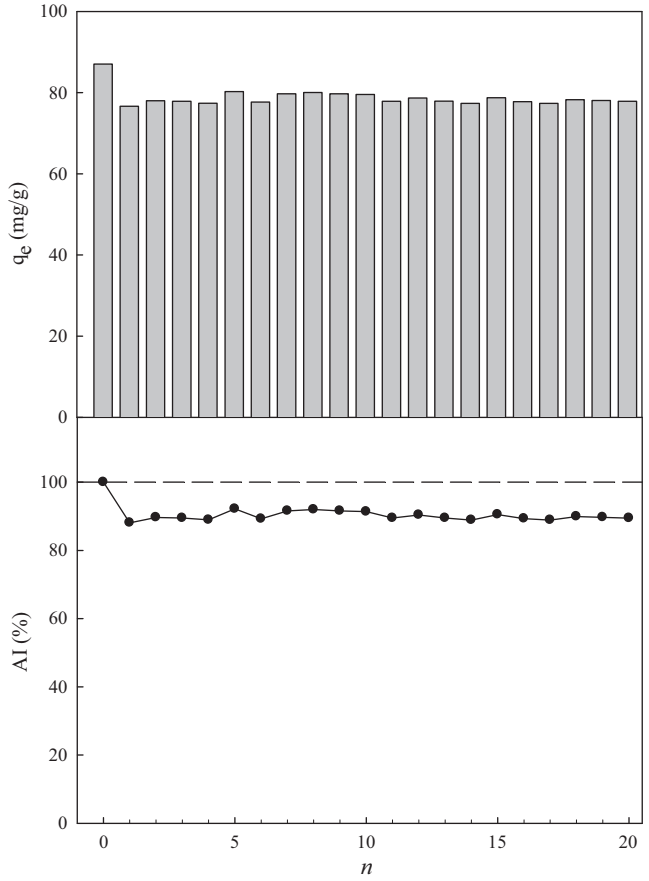

Fig. 11. Cyclic adsorption of 15% CO_2 on TEPA-MSP via a thermal/vacuum desorption.

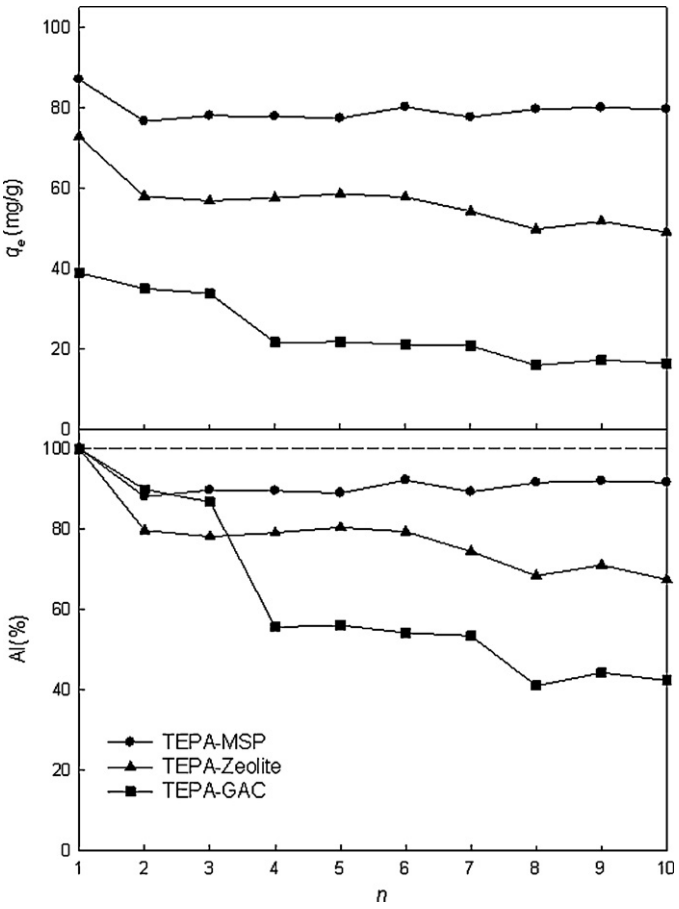

Fig. 12. Comparisons of cyclic adsorption of 15% CO_2 on various adsorbents. (TEPA loaded: 50 wt%.)

the q_e decreased from 87.1 to 78.1 mg/g while the AI decreased from 100 to 89.7% after the first cycle of operation, reflecting that most CO_2 molecules can be effectively desorbed from the surface of TEPA-MSP at 75 °C for 240 min. However, the q_e reached stability and showed below 1% attrition during the following 19 cycles of operation. This suggests that the TEPA-MSP can be employed in the prolonged cyclic CO_2 adsorption through a temperature/vacuum swing operation.

The crystal phase, the TGA, and the surface functional groups of TEPA-MSP after 20 cycles of adsorption and desorption operation are also given in Figs. 6–8. It is observed that the XRD pattern, the TGA profile, and the IR spectrum of regenerated TEPA-MSP display similar trends to those of virgin TEPA-MSP. This reflects that the physicochemical properties of TEPA-MSP were preserved after 20 cycles of operation.

3.5. Comparative study

Fig. 12 displays the q_e and AI of 15% CO_2 adsorption on TEPA-MSP, TEPA-zeolite, and TEPA-GAC at 60 °C. I The q_e decreased from 87.05 to 79.12 mg/g (AI = 90.9%) for TEPA-MSP, 72.87 to 49.82 mg/g (AI = 68.37%) for TEPA-zeolite, and 39.02 to 17.32 mg/g (AI = 44.39%) for GAC-TEPA after 10 cycles of adsorption–desorption operation. The TEPA-MSP showed higher q_e and rather stable AI than the TEPA-zeolite and TEPA-GAC, reflecting that they can be stably employed in the prolonged cyclic CO_2 adsorption via a temperature/vacuum swing operation.

The foregoing results reveals that the 50 wt% TEPA-MSP not only display high adsorption capacity of 15% CO_2 but also show stability in the cyclic CO_2 adsorption. These advantages suggest that adsorption with solid TEPA-MSP is a promising CO_2 capture technology.

4. Conclusions

The MSP were manufactured via a pilot-scale spray drying system and modified with TEPA to study their physicochemical properties and cyclic CO_2 adsorption. The surface nature of MSP were changed after TEPA modification including the increase in affinity between CO_2 molecules and MSP surface and the increase in surface functional groups, which makes the TETA-MSP that adsorb significant amount of CO_2 gases. The CO_2 adsorption capacities and the physicochemical properties of TEPA-MSP were preserved through 20 cycles of adsorption and desorption operation. The TEPA-MSP showed higher adsorption capacity of 15% CO_2 and less attribution than the TEPA-GAC and TEPA-zeolite. These results suggest that the TEPA-MSP can be employed for prolonged cyclic CO_2 adsorption and they possess the potential for CO_2 capture from flue gas.

Acknowledgment

Support from the Bureau of Energy, Ministry of Economic Affairs of Taiwan is gratefully acknowledged.

References

[1] W.H. Liu, H.W. Hsu, J.F. Huang, C.M. Huang, H.C. Wang, Carbon dioxide capture technology plan and development in Taiwan, in: The International Pittsburgh Coal Conference (PCC), 2008.
[2] C.M. White, B.R. Strazisar, E.J. Granite, J.S. Hoffman, H.W. Pennline, J. Air Waste Manage. Assoc. 53 (2003) 645–715.
[3] D. Aaron, C. Tsouris, Sep. Sci. Technol. 40 (2005) 321–348.
[4] M.M. Abu-khader, Energy Source A 28 (2006) 1261–1279.
[5] Intergovernmental Panel on Climate Change (IPCC), Special report on carbon dioxide capture and storage, 2005.
[6] A. Sayari, Y. Belmabkhout, R. Serna-Guerrero, Chem. Eng. J. 171 (2011) 760–774.
[7] A. Samanta, A. Zhao, G.K.H. Shimizu, P. Sarkar, R. Gupta, Ind. Eng. Chem. Res. 51 (2012) 1438–1463.
[8] R.V. Siriwardane, M.S. Shen, E.P. Fisher, J.A. Posten, Energy Fuels 15 (2001) 279–284.
[9] P. Davini, Carbon 40 (2002) 1973–1979.
[10] J. Przepiórski, M. Skrodzewicz, A.W. Morawski, Appl. Surf. Sci. 225 (2004) 235–242.
[11] C. Lu, H. Bai, B. Wu, F. Su, J.F. Hwang, Energy Fuels 22 (2008) 3050–3056.
[12] C. Pevida, M.G. Plaza, B. Arias, J. Fermoso, F. Rubiera, J.J. Pis, Appl. Surf. Sci. 254 (2008) 7165–7172.
[13] J.S. Lee, J.H. Kim, J.T. Kim, J.K. Suh, J.M. Lee, C.H. Lee, J. Chem. Eng. Data 47 (2002) 1237–1242.
[14] P.J.E. Harlick, F.H. Tezel, Sep. Purif. Technol. 37 (2002) 33–60.
[15] W. Gao, D. Butler, D.L. Tomasko, Langmuir 20 (2004) 8083–8089.
[16] C. Maurin, P.L. Llewellyn, R.G. Bell, J. Phys. Chem. B 109 (2005) 16084.
[17] K.S. Walton, M.B. Abney, M.D. Levan, Micropor. Mesopor. Mater. 91 (2006) 78.
[18] E. Diaz, E. Munoz, A. Vega, S. Ordonez, Ind. Eng. Chem. Res. 47 (2008) 412–418.
[19] R. Chatti, A.K. Bansiwal, J.A. Thote, V. Kumar, P. Jadhav, S.K. Lokhande, R.B. Biniwale, N.K. Labhsetwar, S.S. Rayalu, Micropor. Mesopor. Mater. 121 (2009) 84–89.
[20] F. Su, C. Lu, S.C. Kuo, W. Zeng, Energy Fuels 24 (2010) 1441–1448.
[21] A.R. Millward, O.M. Yaghi, J. Am. Chem. Soc. 127 (2005) 17998–17999.
[22] Y.S. Bae, K.L. Mulfort, H. Frost, P. Ryan, S. Punnathanam, L.J. Broadbelt, J.T. Hupp, R.Q. Snurr, Langmuir 24 (2008) 8592–8598.
[23] V. Finsy, L. Ma, L. Alaert, D.E. de Vos, C.V. Baron, J.F.M. Denayer, Micropor. Mesopor. Mater. 120 (2009) 221–227.
[24] Z. Zhao, Z. Li, Y.S. Lin, Ind. Eng. Chem. Res. 48 (2009) 10015–10020.
[25] J.R. Li, R.J. Kuppler, H.C. Zhou, Chem. Soc. Rev. 38 (2009) 1477–1504.
[26] M. Cinke, J. Li, C.W. Bauschlicher Jr., A. Ricca, M. Meyyappan, Chem. Phys. Lett. 376 (2003) 761–766.
[27] F. Su, C. Lu, W. Chen, H. Bai, J.F. Hwang, Sci. Total Environ. 407 (2009) 3017–3023.
[28] S. Hsu, C. Lu, F. Su, W. Zeng, W. Chen, Chem. Eng. Sci. 65 (2010) 1354–1361.
[29] F. Su, C. Lu, H.S. Chen, Langmuir 27 (2011) 8090–8098.
[30] A.K. Mishra, S. Ramaprabhu, J. Mater. Chem. 22 (2012) 3708–3712.
[31] H.Y. Huang, R.T. Yang, D. Chinn, C.L. Munson, Ind. Eng. Chem. Res. 42 (2003) 2427–2433.
[32] X. Xu, C. Song, J.M. Andresen, B.G. Miller, A.W. Scaroni, Micropor. Mesopor. Mater. 62 (2003) 29–45.
[33] X. Xu, C. Song, B.G. Miller, A.W. Scaroni, Ind. Eng. Chem. Res. 44 (2005) 8113–8119.

[34] M.L. Gray, Y. Soong, K.J. Champagne, H. Pennline, J.P. Baltrus, R.W. Stevens Jr., R. Khatri, S.S.C. Chuang, T. Filburn, Fuel Proc. Technol. 86 (2005) 1449–1455.
[35] N. Hiyoshi, K. Yogo, T. Yashima, Micropor. Mesopor. Mater. 84 (2005) 357–365.
[36] G.P. Knowles, S.W. Delaney, A.L. Chaffee, Ind. Eng. Chem. Res. 45 (2006) 2626–2633.
[37] R. Serna-Guerrero, E. Da'na, A. Sayari, Ind. Eng. Chem. Res. 47 (2008) 9406–9412.
[38] M.B. Yue, L.B. Sun, Y. Cao, Z.J. Wang, Y. Wang, Q. Yu, J.H. Zhu, Micropor. Mesopor. Mater. 114 (2008) 74–81.
[39] C. Lu, F. Su, S. Hsu, W. Chen, H. Bai, J.F. Hwang, H.H. Lee, Fuel Process. Technol. 90 (2009) 1543–1549.
[40] C. Lu, H. Bai, F. Su, W. Chen, J.F. Hwang, H.H. Lee, J. Air Waste Manage. Assoc. 60 (2010) 489–496.
[41] S.H. Liu, Y.C. Lin, H.R. Hyu, J. Air Waste Manage. Assoc. 61 (2011) 226–233.
[42] X. Ji, Q. Hu, J.E. Hampsey, X. Qiu, L. Gao, J. He, Y. Lu, Chem. Mater. 18 (2006) 2265–2274.
[43] R. Pitchumani, J.J. Heiszwolf, A. Schmidt-Ott, M.O. Coppens, Micropor. Mesopor. Mater. 120 (2009) 39–46.
[44] M. Ide, E. Wallaert, I.V. Driessche, F. Lynen, P. Sandra, P.V.D. Voort, Micropor. Mesopor. Mater. 142 (2011) 282–291.
[45] C.T. Hung, H. Bai, Chem. Eng. Sci. 63 (2008) 1997–2005.
[46] C.T. Hung, H. Bai, M. Karthik, Sep. Purif. Technol. 64 (2009) 265–272.
[47] A.L. Chaffee, G.P. Knowles, Z. Liang, J. Zhang, P. Xiao, P.A. Webley, Int. J. Greenhouse Gas Control 1 (2007) 11–18.
[48] A. Bosoaga, O. Masek, J.E. Oakey, Energy Procedia 1 (2009) 133–140.
[49] C.C. Cormos, F. Starr, E. Tzimas, S. Peteves, Int. J. Hydrogen Energy 33 (2008) 1286–1294.
[50] Y. Yamauchi, N. Suzuki, L. Radhakrishan, L. Wang, Chem. Rec. 9 (2009) 321–339.
[51] I.W. Lenggoro, T. Hata, F. Iskandar, J. Mater. Res. 15 (2000) 733–743.
[52] S.J. Gregg, K.S.W. Sing, Adsorption Surface Area and Porosity, Academic Press, New York, 1982.
[53] C.T. Hsieh, Y.W. Chou, Sep. Sci. Technol. 41 (2006) 3155–3168.
[54] M.B. Yue, L.B. Sun, Y. Cao, Y. Wang, Z.J. Wang, J.H. Zhu, Chem. Eur. J. 14 (2008) 3442–3451.
[55] F. Zheng, D.N. Tran, B.J. Busche, G.E. Fryxell, R.S. Addleman, T.S. Zwmanian, C.L. Aardahl, Ind. Eng. Chem. Res. 44 (2005) 3099–3105.
[56] X. Wang, V. Schwartz, J.C. Clark, X. Ma, S. Overbury, X. Xu, C. Song, J. Phys. Chem. C 113 (2009) 7260–7268.
[57] A.C.C. Chang, S.S.C. Chuang, M. Gray, Y. Soong, Energy Fuels 17 (2003) 468–473.
[58] X. Xu, C. Song, B.G. Miller, A.W. Scaroni, Fuel Proc. Technol. 86 (2005) 1457–1472.